

We are IntechOpen, the world's leading publisher of Open Access books Built by scientists, for scientists

6,900

Open access books available

186,000

International authors and editors

200M

Downloads

Our authors are among the

154

Countries delivered to

TOP 1%

most cited scientists

12.2%

Contributors from top 500 universities



WEB OF SCIENCE™

Selection of our books indexed in the Book Citation Index
in Web of Science™ Core Collection (BKCI)

Interested in publishing with us?
Contact book.department@intechopen.com

Numbers displayed above are based on latest data collected.
For more information visit www.intechopen.com



Heat Transfer Correlations of Supercritical Fluids

Fangbo Li, Binbin Pei and Bofeng Bai

Abstract

The drastic changes of thermophysical properties in the pseudo-critical region of supercritical fluids bring very big challenges to the traditional Dittus-Boelter-type heat transfer correlations. In this chapter, we will talk about the principles and applications of two kinds of heat transfer correlations of supercritical fluids: the empirical type and the semiempirical type. For the empirical correlations, the modification methods taking into account the variable properties and body force effects will be introduced. We will focus on the proposal of nondimensional parameters describing the buoyancy effect and flow acceleration; while for the semiempirical ones, we mainly talk about the new kind of correlation which is based on the momentum and energy conservations in the mixed convective flow.

Keywords: heat transfer correlation, empirical type, semiempirical type, buoyancy effect, flow acceleration

1. Introduction

Establishing an accurate heat transfer correlation of supercritical fluid is the prerequisite of the design of the apparatus and devices, such as the supercritical boilers, generation IV reactors, and heat exchangers [1–4]. However, the drastic change of the thermodynamic properties in the pseudo-critical region and the complex mechanism of turbulent heat transfer lead to difficulties in predicting the heat transfer performance accurately. There are three distinguished heat transfer regimes for supercritical fluid: normal heat transfer (normal HT), improved heat transfer (improved HT), and deteriorated heat transfer (deteriorated HT). The normal HT regime is characterized by the heat transfer coefficients similar with those predicted by the Dittus-Boelter (DB) correlation at subcritical condition; the improved HT regime can be characterized by the higher heat transfer coefficients and lower wall temperatures compared with the normal HT; and the deteriorated HT regime is accompanied with lower heat transfer coefficients than the normal HT; hence, the wall temperature peak can be observed. **Figure 1** illustrates the heat transfer performances of supercritical CO₂ under different mass fluxes and heat fluxes [5] of the upward flow in a circular tube with an inner diameter of 6.32 mm and heated length of 2.65 m. At relatively lower heat flux/mass flux ratio, the heat transfer will be obviously improved due to the large specific heat in the

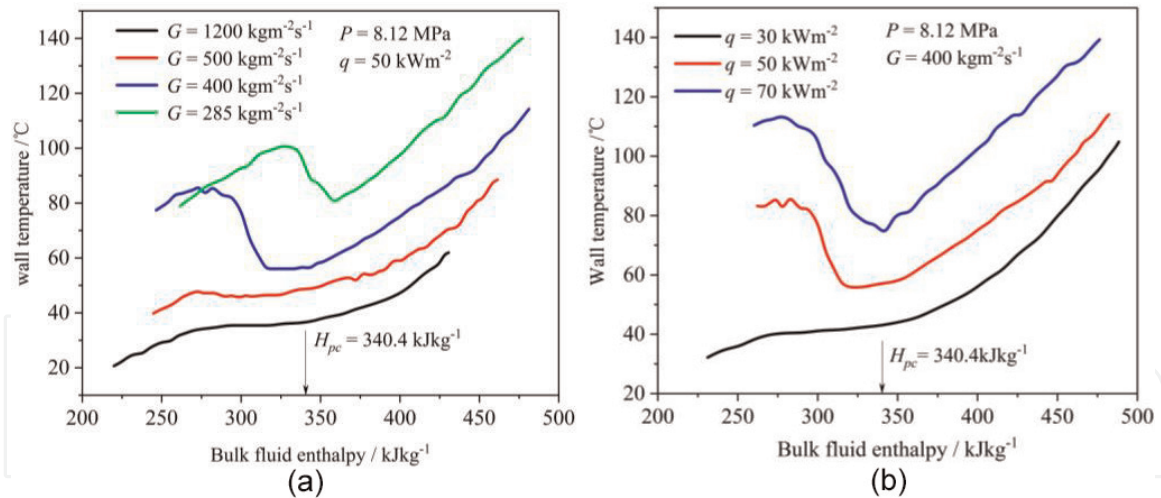


Figure 1.

Heat transfer performances of supercritical CO₂ of the upward flow under different (a) mass fluxes and (b) heat fluxes in a circular tube with an inner diameter of 6.32 mm and heated length of 2.65 m. Symbols: G , mass fluxes ($\text{kg m}^{-2} \text{s}^{-1}$); P , pressure (MPa); q , wall heat flux (kW m^{-2}); H , enthalpy (kJ kg^{-1}). Data in this figure come from Ref. [1].

pseudo-critical region. The heat transfer coefficients will be higher than the ones calculated by the Dittus-Boelter correlation. As the heat flux/mass flux ratio increases, the mixing convective heat transfer occurs, and the wall temperature peak caused by the heat transfer deterioration can be observed. The experiment conducted by Kurganov and Kaptil'ny [6] offered an insight into the mechanism of heat transfer deterioration, the M-shaped velocity profile was observed, and it was considered to be closely associated with the flattened velocity gradient, reduced turbulent shear stress, and turbulent kinetic energy due to the body force (also known as the buoyancy effect). Bae et al. [7, 8] obtained the budgets of the turbulent kinetic energy in the deteriorated heat transfer by using direct numerical simulation, and the mechanism of buoyancy and flow acceleration were analyzed.

The heat transfer correlations are established on the basis of heat transfer mechanism, and a vast majority of correlations are intended for use only for normal HT and improved HT regimes. They can be categorized into two types: the empirical type and the semiempirical type. In the empirical correlations, the correction terms composed of different thermophysical properties (such as the density, thermal conductivity, specific heat, and viscosity) are introduced to the heat transfer correlation of the constant-property fluid (i.e., DB correlation) [9]. However, the performance of the empirical correlations deteriorates with the increasing of the heat flux/mass flux ratio; thus, the empirical correlations considering the nondimensional numbers which reflect the buoyancy and thermally induced flow acceleration effects have also been proposed [10]. It is shown that the predictions on the mixing convection cases can be improved by this method. In order to further improve the performances of the empirical correlations under the strong buoyancy effect, some researchers tried to establish the semiempirical correlations based on the theoretical analysis approaches [11, 12]. The existing semiempirical correlations mainly aim to derive the qualitative relationship between the heat transfer impairment and turbulent shear stress reduction; the coefficients appeared in the correlation are obtained by fitting the experimental data.

In this chapter we mainly talk about the heat transfer correlations of supercritical fluid. Both the empirical type and the semiempirical type will be introduced here. We mainly focus on the principles, applications, and comparisons of these correlations.

2. Empirical heat transfer correlations

For the improved HT and normal HT regimes, abundant empirical correlations have been proposed, and most of them can give satisfying predictions [13–15]. Morky et al. [9] and Gupta et al. [16] proposed the correlations based on the Buckingham Π theorem, and the comparison with the experimental results confirmed their capability on the calculating the heat transfer improvement regime. However, as the increasing of the heat flux, the effect of the mixing convection increases. The fluid near the heated wall is accelerated under the effect of the buoyancy force and the flow acceleration, leading to the attenuation of heat transfer [17]. On the basis of this, researchers tried to modify the correlations by considering the nondimensional numbers reflecting the buoyancy force and the flow acceleration. Bae and Kim [10] and Komita et al. [18] analyzed the momentum balance under the mixed convection case and proposed a nondimensional parameter Bu to describe the effect of the buoyancy on the shear stress; then, they proposed a new function to describe the relationship between the Nusselt numbers and Bu based on the experimental data. This heat transfer correlation takes the form of the piecewise function divided by the value of the Bu number. Deev et al. [19] discussed the heat transfer of supercritical water in the channel. Two nondimensional criteria considering the effects of the viscous force and inertial force on heat transfer were proposed, and the weight constant treating the superposition between the forced and natural convection was introduced. Such practices were also conducted by Cheng et al. [20], Yu et al. [21], and Kuang et al. [22]. In their work, the dimensionless numbers such as the buoyancy number and the acceleration number were proposed to correct the deviation of the real heat transfer from that of the normal HT regime. **Figure 2** shows the approach establishing the empirical correlations. The dimensionless groups are firstly chosen, and the coefficients in the correlation can be obtained by the linear regression analysis. Through variable transformations the dimensionless groups are reduced, and the final form can be obtained. Some typical empirical correlations are listed in **Table 1**.

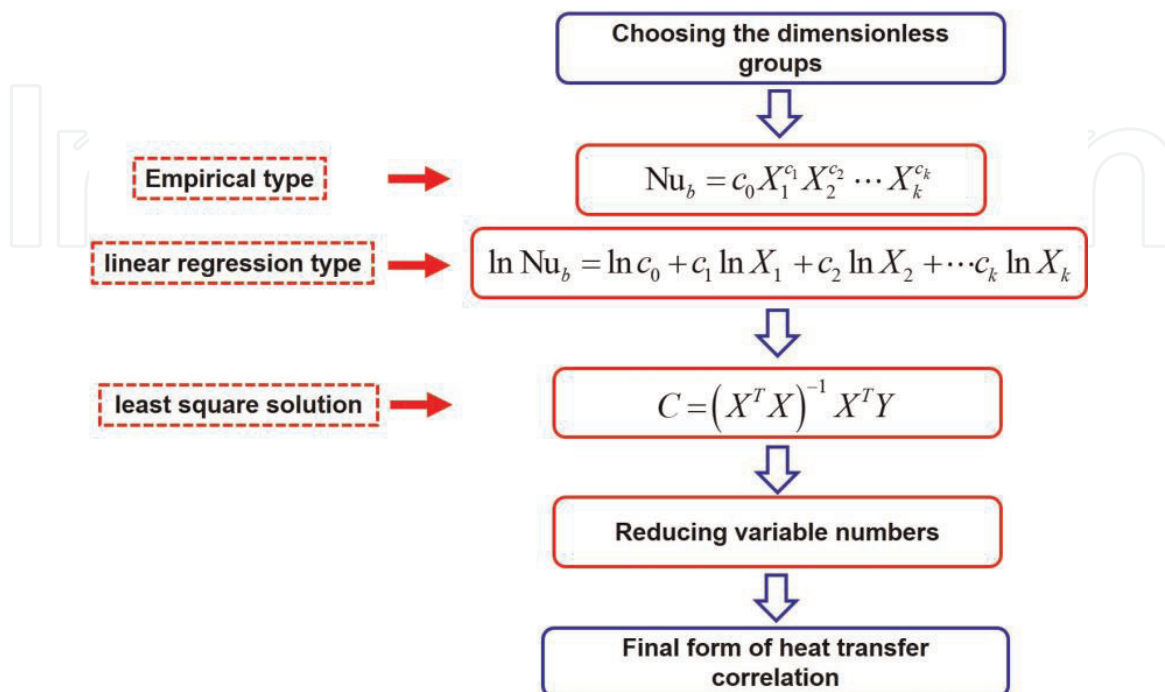


Figure 2.
 The approach deriving the empirical correlations.

Ref.	Fluid	Parameters range	Correlation
Mokry et al. [9]	H ₂ O	$P = 22.8\text{--}29.4$ MPa $G = 200\text{--}1500$ kg m ⁻² s ⁻¹ $q = 70\text{--}1250$ kW m ⁻² $d = 3\text{--}38$ mm	$\text{Nu}_b = 0.0061 \text{Re}_b^{0.914} \overline{\text{Pr}}_b^{-0.654} (\rho_w/\rho_b)^{0.518}$ $\overline{\text{Pr}}_b = \frac{\overline{c_p} \mu_b}{\lambda_b}, \overline{c_p} = \frac{H_w - H_b}{T_w - T_b}$
Gupta et al. [16]	H ₂ O	$P = 24$ MPa $G = 200\text{--}1500$ kg m ⁻² s ⁻¹ $q = 70\text{--}1250$ kW m ⁻²	$\text{Nu}_w = 0.004 \text{Re}_w^{0.923} \overline{\text{Pr}}_w^{0.773}$ $(\mu_w/\mu_b)^{0.366} (\rho_w/\rho_b)^{0.186}$
Jackson [23]	H ₂ O	After review of the existing literatures and data	$\text{Nu}_b = 0.0183 \text{Re}_b^{0.82} \text{Pr}_b^{0.5} (\rho_w/\rho_b)^{0.3} (\overline{c_p}/c_{pb})^n$ where the exponent n is taken as i. $n = 0.4 + 0.2(T_w/T_{pc} - 1)(1 - 5(T_b/T_{pc} - 1))$ for $T_{pc} < T_b < 1.2T_{pc}$; ii. $n = 0.4 + 0.2(T_w/T_{pc} - 1)$ for $T_b < T_{pc} < T_w$; iii. $n = 0.4$ for $T_b < T_w < T_{pc}$ and $1.2T_{pc} < T_b < T_w$.
Bae and Kim [10]	CO ₂	$P = 7.75\text{--}8.55$ MPa $G < 1200$ kg m ⁻² s ⁻¹ $q_w < 150$ kW m ⁻²	$\text{Nu}_b = \text{Nu}_{\text{varp}} f(\text{Bu}) \text{Nu}_{\text{varp}} = 0.021 \text{Re}_b^{0.82} \text{Pr}_b^{0.5} (\rho_w/\rho_b)^{0.3} (\overline{c_p}/c_{pb})^n$ i. For $5 \times 10^{-8} < \text{Bu} < 7 \times 10^{-7}$, $f(\text{Bu}) = (1 + 10^8 \text{Bu})^{0.032}$ ii. For $7 \times 10^{-7} < \text{Bu} < 1 \times 10^{-6}$, $f(\text{Bu}) = 0.0185 \text{Bu}^{-0.435}$ iii. $1 \times 10^{-6} < \text{Bu} < 1 \times 10^{-5}$, $f(\text{Bu}) = 0.75$ iv. For $1 \times 10^{-5} < \text{Bu} < 3 \times 10^{-5}$, $f(\text{Bu}) = 0.0119 \text{Bu}^{-0.36}$ v. For $3 \times 10^{-5} < \text{Bu} < 1 \times 10^{-4}$, $f(\text{Bu}) = 32.4 \text{Bu}^{0.4}$
Cheng et al. [20]	H ₂ O	$d = 10, 20$ mm $P = 22.5\text{--}25$ MPa $G < 3500$ kg m ⁻² s ⁻¹ $q_w < 2000$ kW m ⁻² $T_b = 300\text{--}450^\circ\text{C}$	$\text{Nu}_b = 0.023 \text{Re}_b^{0.8} \text{Pr}_b^{1/3} F$ $F = \min(F_1, F_2)$ $F_1 = 0.85 + 0.776(10^3 \pi_A)^{2.4}$ $F_2 = \frac{0.48}{(10^3 \pi_{A,pc})^{1.55}} + 1.21 \left(1 - \frac{\pi_A}{\pi_{A,pc}}\right)$ $\pi_A = \frac{\beta q}{c_p G}$
Deev et al. [19]	H ₂ O	$d = 2.67\text{--}12.0$ mm $P = 22.6\text{--}26$ MPa $G < 2000$ kg m ⁻² s ⁻¹ $q_w = 200\text{--}2250$ kW m ⁻²	$\text{Nu}_b = 0.023 \text{Re}_b^{0.8} \text{Pr}_b^{0.4} (\rho_w/\rho_b)^{0.25} (\overline{c_p}/c_{pb})^n Y Y = (1 - \xi) Y_1 + \xi Y_2$ $Y_1 = 1 + a_1 \exp(b_1 K_h^2 + c_1 K_h)$ $Y_2 = 1 + a_2 \exp(b_2 K_h^2 + c_2 K_h)$ $\zeta = \exp(-0.5(K_{Am})^2)$ $K_h = K_{Am}(H_b - H_{pc})/H_{pc}$

Ref.	Fluid	Parameters range	Correlation
			$a_1 = 1.5, b_1 = -30, c_1 = 3$ $a_2 = -0.15, b_2 = -125, c_2 = -25$ $K_{Am} = (10^{-5} Re_{pc})^{0.5} / (10^3 K_{qm})$ $K_{qm} = q_w \beta_{pc} / (G c_{p,pc})$
Yu et al. [21]	H ₂ O	After review of the existing literatures and data	$Nu_b = 0.01378 Re_b^{0.9078} \overline{Pr}_b^{0.6171}$ $(\rho_w / \rho_b)^{0.4356} (Gr^*)^{-0.012} (q^+)^{0.0605}$ $\overline{Pr}_b = \frac{\overline{c}_p \mu_b}{\lambda_b}, \overline{c}_p = \frac{H_w - H_b}{T_w - T_b},$ $Gr^* = \frac{g \beta d^4 q_w}{\lambda_b \nu_b^2}, q^+ = \frac{\beta q_w}{G c_p}$
Kuang et al. [22]	H ₂ O	After review of the existing literatures and data	$Nu_b = 0.0239 Re_b^{0.759} \overline{Pr}_b^{0.833} (\rho_w / \rho_b)^{0.31} (\lambda_w / \lambda_b)^{0.0863}$ $(\mu_w / \mu_b)^{0.832} (Gr^*)^{0.014} (q^+)^{-0.021}$ $\overline{Pr}_b = \frac{\overline{c}_p \mu_b}{\lambda_b}, \overline{c}_p = \frac{H_w - H_b}{T_w - T_b},$ $Gr^* = \frac{g \beta d^4 q_w}{\lambda_b \nu_b^2}, q^+ = \frac{\beta q_w}{G c_p}$

Table 1.
Typical empirical heat transfer correlations of supercritical fluids.

3. Semiempirical heat transfer correlations

As is mentioned before, as the heat flux increases, the heat transfer deterioration phenomenon will happen. Heat transfer deterioration is characterized with lower values of the heat transfer coefficients and very high wall temperatures. A widely used quantitative expression to define the heat transfer deterioration of supercritical fluid [24–26] is shown by Eq. (1):

$$h < c \cdot h_{DB} = c \cdot 0.023 \frac{\lambda_b}{d} \text{Re}_b^{0.8} \text{Nu}_b^{0.4} \quad (1)$$

where h refers to the heat transfer coefficient of the heat transfer deterioration and h_{DB} is the heat transfer coefficient given by the Dittus-Boelter correlation (i.e., normal HT regime). The coefficient c is taken as 0.3 by Schatte et al. [24]. Unfortunately, under the deteriorated HT regime, most of the empirical correlations will lose their accuracy. When deteriorated HT regime occurs, the dominated mechanism of the turbulent heat transfer is the interaction among the buoyancy, flow acceleration, and variable thermophysical properties. Unfortunately the empirical correlations can hardly reflect the heat transfer mechanism. Thus, their performances are unsatisfying, as is shown in **Figure 3**.

3.1 Correlation by Jackson

Jackson [12] investigated the semiempirical correlation considering the effect of the mixed convective heat transfer in a vertical heated tube. The author proposed an equivalent “buoyancy-free forced convective flow” which has the same heat transfer effect with the real supercritical fluid flow. He tried to establish the relationship between the heat transfer coefficients attenuation and the shear stress reduction based on the equivalent Nusselt and Reynolds numbers of the equivalent flow with the aid of the empirical equation under forced convective condition. Integrating the equations of momentum across the entire flow and the near-wall layer of thickness δ_t , respectively, then reorganizing the two equations leads to

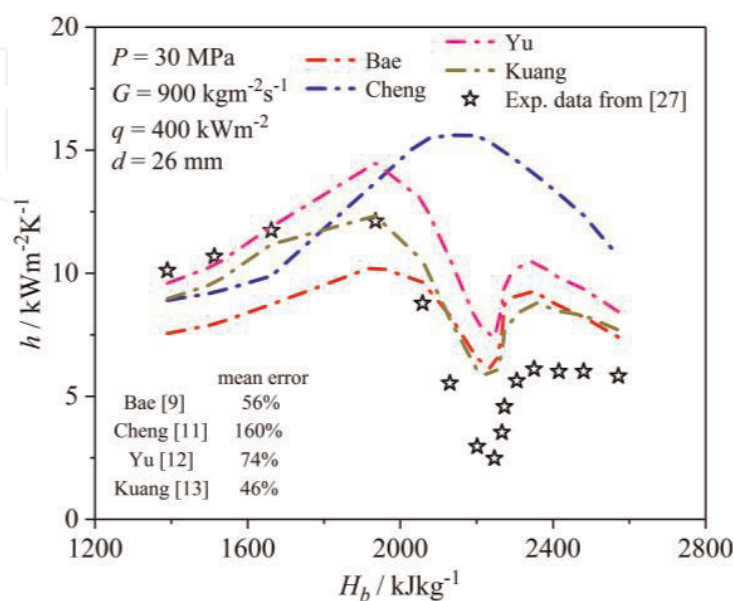


Figure 3.

The comparison among the results of the empirical correlations listed in **Table 1** and the experimental results from Hu [27]. This case describes the upward flow of supercritical water in a circular tube with an inner diameter of 26 mm and heated length of 2.0 m. Data in this figure come from Ref. [11].

$$\tau_w - \tau_{\delta_t} = \pm \delta_t (\rho_b - \rho_{ave}) g \quad (2)$$

where τ_w is the wall shear stress, τ_{δ_t} is the shears stress at $y = \delta_t$, and the integrated average value of the density ρ_{ave} across the near-wall layer is defined by $\rho_{ave} = \int_0^{\delta_t} \rho dy / \delta_t$. In Eq. (2) the positive sign indicates the upward flow, and the negative one is applied for the downward flow. Then the author assumed that the effect of the buoyancy in modifying the distribution of shear stress and turbulence production has led to such an “equivalent” flow which is not influenced by the buoyancy but has a bulk velocity which is either higher or lower than the real flow. The wall shear stress τ'_w for this “equivalent” buoyancy-free flow can be replaced by the modified shear stress τ_{δ_t} at the location $y = \delta_t$ in a turbulent shear flow. Then the author proposed a model which reflects the shear stress distributions in the supercritical fluid flow:

$$\tau_{\delta_t} / \tau_w = (\text{Re}'_b / \text{Re}_b)^{2-m_1} (F'_{VP1} / F_{VP1}) \quad (3)$$

where the F'_{VP1} and F_{VP1} are the modifications on the variable properties for the “equivalent” buoyancy-free flow and the real flow, respectively. The Nusselt number of the “equivalent” forced convection can be expressed in terms of the Reynolds number, Re'_b , using the empirical equation:

$$\text{Nu}_B = K_2 (\text{Re}'_b)^{m_2} \text{Pr}_b^{n_2} F'_{VP2} \quad (4)$$

where K is the constant and then

$$\text{Nu}_F = K_2 \text{Re}_b^{m_2} \text{Pr}_b^{n_2} F_{VP2} \quad (5)$$

Combining Eqs. (4) and (5) follows that

$$\text{Nu}_B / \text{Nu}_F = (\text{Re}'_b / \text{Re}_b)^{m_2} (F'_{VP2} / F_{VP2}) \quad (6)$$

Combining Eqs. (2) and (5) the author obtained

$$\text{Nu}_B / \text{Nu}_F = [(F'_{VP2} / F_{VP1})^{m_4} / (F_{VP2} / F_{VP1})^{m_4}] (\tau_{\delta_t} / \tau_w)^{m_4} \quad (7)$$

Or equivalently

$$\text{Nu}_B = K_2 \text{Re}_b^{m_2} \text{Pr}_b^{n_2} F_{VP2} (F'_{VP3} / F_{VP3}) (\tau_{\delta_t} / \tau_w)^{m_4} \quad (8)$$

The above equation shows the relationship between the heat transfer and the reduced shear stress across the near-wall layer. Based on this, the author considered three cases of mixing convective heat transfer in a vertical heated tube to fluid flowing either in the upward direction (i.e., the buoyancy-aided case) or the downward direction (i.e., the buoyancy-opposed case). Firstly, a model of the buoyancy-influenced heat transfer was proposed:

$$\left(\frac{\text{Nu}_B}{\text{Nu}_F} \right) \left(\frac{F_{VP3}}{F'_{VP3}} \right) = \left[\left[1 \mp (C_B \text{Bo}_b^* F_{VPB}) \left[\left(\frac{\text{Nu}_B}{\text{Nu}_F} \right) \left(\frac{F_{VP3}}{F'_{VP3}} \right) \right]^{-2.1} \right] \right]^{0.45} \quad (9)$$

where C_B is a constant, Bo_b is the buoyancy number, and F_{VPB} is the modification on the variable properties for the buoyancy-influenced flow. As can be seen from Eq. (9), $(\text{Nu}_B / \text{Nu}_F) (F_{VP3} / F'_{VP3})$ is a unique function of a single parameter

$(C_B Bo_b^* F_{VPB})$, and the author referred to this function as $\psi(C_B Bo_b^* F_{VPB})$. It can be evaluated by assigning a series of values to the product $(C_B Bo_b^* F_{VPB})$ in Eq. (9) and calculating the corresponding values of $(Nu_B/Nu_F)(F_{VP3}/F'_{VP3})$. **Figure 4(a)** shows the effect of the buoyancy on heat transfer predicted by Eq. (9) by the three curves (the red line for the downward flow and the black line for the upward flow). Note that by **Figure 4(a)**, we can see if $(C_B Bo_b^* F_{VPB})$ is less than 0.04, the function $\psi(C_B Bo_b^* F_{VPB})$ will be within about 2% of unity; thus, the heat transfer mode will be the variable-property forced convective heat transfer.

The second model proposed by the author was about the heat transfer due to the thermally induced flow acceleration. It shows how the acceleration of a heated flow causes the reduced turbulence production, the deteriorated HT, and the turbulence laminarization. The final form of this model is given as

$$\left(\frac{Nu_A}{Nu_F}\right)\left(\frac{F_{VP3}}{F'_{VP3}}\right) = \left[1 - (C_A Ac_b F_{VPA}) \left[\left(\frac{Nu_B}{Nu_F}\right)\left(\frac{F_{VP3}}{F'_{VP3}}\right)\right]^{-1.1}\right]^{0.45} \quad (10)$$

where C_A is a constant, Ac_b is the flow acceleration number, and F_{VPA} is the modification on the variable properties for the acceleration-influenced flow. As is shown in Eq. (10), the product $(Nu_A/Nu_F)(F_{VP3}/F'_{VP3})$ is a unique function of the parameter $(C_A Ac_b F_{VPA})$, and we will describe this function as $\psi(C_A Ac_b F_{VPA})$. The variation of $\psi(C_A Ac_b F_{VPA})$ with $(C_A Ac_b F_{VPA})$ can be readily determined using a similar approach to that described in the buoyancy-influenced heat transfer case. The result is shown in **Figure 4(b)**. The function $\psi(C_A Ac_b F_{VPA})$ is predicted to fall from unity as $(C_A Ac_b F_{VPA})$ increases from zero. This indicates that the heat transfer is attenuated as the flow acceleration increases, and note that this phenomenon is independent on the flow direction. The author argued that with the increase of the flow acceleration, the excess pressure acting on the flow is able to balance the shear stress; thus, the core layer will not experience any shear stress and soon leads to the turbulence laminarization.

The third model was presented which describes the heat transfer under the condition where the influence of the buoyancy and the thermally induced bulk flow acceleration are combined together. Using the approach developed earlier to relate the Nusselt number ratio and the shear stress ratio, the author proposed

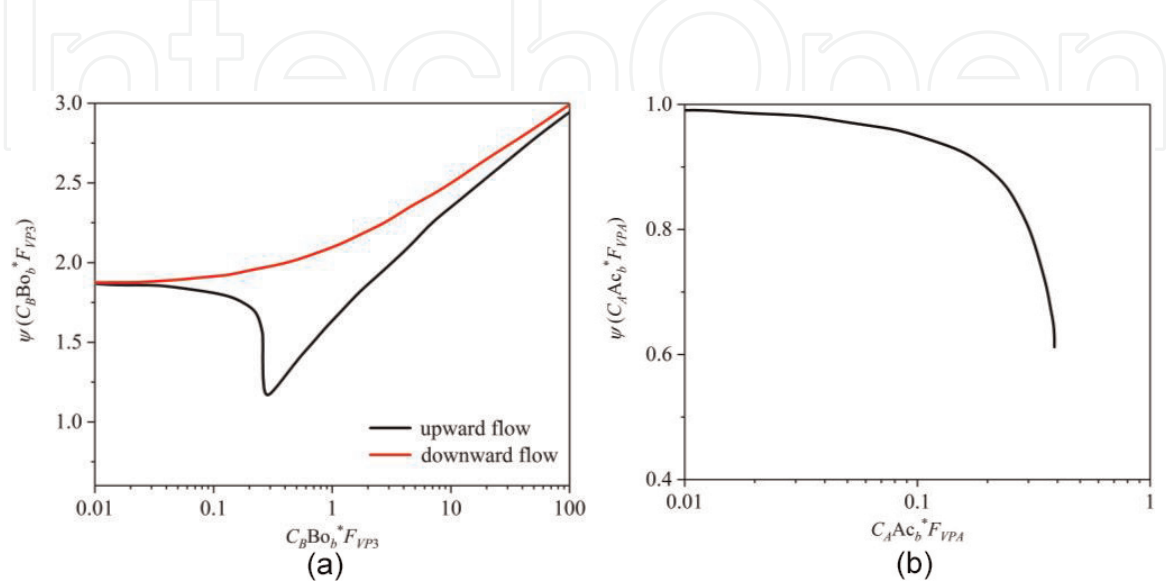


Figure 4. Effect of the theoretical buoyancy and flow acceleration factors on heat transfer [12], (a) the effect of buoyancy, and (b) the effect of flow acceleration. Data in this figure come from Ref. [12].

$$\left(\frac{\text{Nu}_{BA}}{\text{Nu}_F}\right)\left(\frac{F_{VP3}}{F'_{VP3}}\right)^{-1.1} = \left[1 \mp (C_B \text{Bo}_b^* F_{VPB}) \left(\frac{\text{Nu}_{BA}}{\text{Nu}_F}\right)^{-2.1} \left(\frac{F_{VP3}}{F'_{VP3}}\right)^{-2.1} - r (C_B \text{Bo}_b^* F_{VPB}) \left(\frac{\text{Nu}_{BA}}{\text{Nu}_F}\right)^{-2.1} \left(\frac{F_{VP3}}{F'_{VP3}}\right)^{-2.1}\right]^{0.45} \quad (11)$$

Here the parameter r indicates the ratio of $(\text{Nu}_{BA}/\text{Nu}_F)^{-1.1} (C_A \text{Ac}_b F_{VPA})$ to $(\text{Nu}_{BA}/\text{Nu}_F)^{-2.1} (C_B \text{Bo}_b^* F_{VPB})$ (i.e., the ratio of the strengths of the buoyancy effect to the flow acceleration effect). In **Figure 5**, the author evaluated the parameter $(\text{Nu}_{BA}/\text{Nu}_F) (F_{VP3}/F'_{VP3})$ for the specified values of $(C_B \text{Bo}_b^* F_{VPB})$ and r and produced the curves of $\phi_{BA} (C_B \text{Bo}_b^* F_{VPB}) = (\text{Nu}_{BA}/\text{Nu}_F) (F_{VP3}/F'_{VP3})^{-1.1}$ against $(C_B \text{Bo}_b^* F_{VPB})$ and r . Thus, for the upward flow, the acceleration influence promotes the buoyancy effect, whereas for the downward flow, the acceleration opposes the buoyancy effect. These trends are illustrated in **Figure 5** for three values of $r = 0, 0.5, \text{ and } 0.8$.

3.2 Correlation by Li and Bai

Li and Bai [11] proposed a semiempirical correlation based on the momentum and energy integration equations in the thermal boundary layer. The authors observed the direct numerical simulation (DNS) data under deteriorated HT regime in Bae et al. [7], Hu [27], Peeters et al. [28], and Zhang et al. [29], and they found that in the turbulent core, the temperature gradient is negligible; therefore, the fluid temperature in the core is approximately the bulk temperature, especially when $T_b < T_{pc} < T_w$. While in the thermal boundary layer δ , the fluid temperature increases from T_b to T_w (where δ is the thickness of the thermal boundary layer). This can be explained as follows: the fluid within the pseudo-critical region absorbs considerable energy due to the high c_p , leading to the small temperature gradient in the turbulent core [7]. Based on these characteristics, Li and Bai built a “two-layer model” for deteriorated HT (as is shown in **Figure 6**) [11, 30]. The turbulence in the tube is divided into two layers: the thermal boundary layer and the core layer. In the thermal boundary layer, the buoyancy is strong and leads to the shear stress

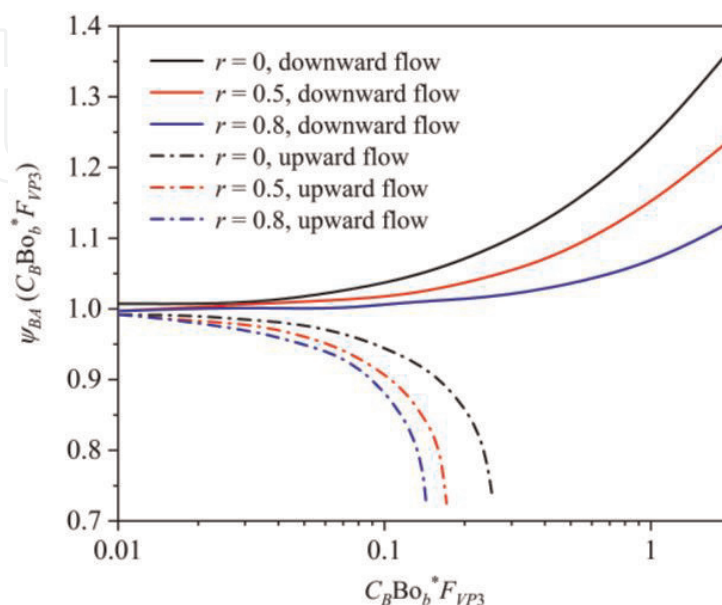


Figure 5. Heat transfer for mixed flow with combined influence of flow acceleration and buoyancy effect [12]. Data in this figure come from Ref. [12].

redistribution. However, in the core layer, the temperature and density gradients are small; hence, the buoyancy effect can be neglected.

Figure 6 shows the straight tube the authors analyzed, and the flow direction is vertically upward. As is shown, the element $abcd$ with a thickness of δ and a length of dx in the thermal boundary layer is chosen to build up the momentum equation:

$$-\frac{dp}{dx} - \frac{\tau_w}{\delta} + \frac{\tau_\delta}{\delta} - \bar{\rho}g = \frac{1}{\delta} \frac{d}{dx} \left(\int_0^\delta \rho u^2 dy \right) \quad (12)$$

In the above equation, τ_w is the shear stress at the wall and $\bar{\rho}$ is the average density across the thermal boundary layer. The wall shear stress and friction factor here are calculated based on Blasius equation, as is shown in Eqs. (13) and (14):

$$\tau_w = 0.5 f_b \rho_b u_b^2 \quad (13)$$

$$f_b = 0.079 \text{Re}_b^{-0.25} \quad (14)$$

Assume that the pressure gradient on the cross section keeps constant. In a similar way, for the bulk flow, we could get

$$-\frac{dp}{dx} - \frac{2\tau_w}{R} - \rho_b g = (\rho u)_b \frac{du_b}{dx} = G \frac{du_b}{dx} \quad (15)$$

Subtracting Eq. (15) and Eq. (12), the pressure gradient could be eliminated and the following result could be obtained:

$$\frac{2\tau_w}{R} - \frac{\tau_w - \tau_\delta}{\delta} + (\rho_b - \bar{\rho})g = \frac{1}{\delta} \frac{d}{dx} \left(\int_0^\delta \rho u^2 dy \right) - G \frac{du_b}{dx} \quad (16)$$

It is obvious that for the vertically upward flow, the radial part of the velocity (u_r) is small enough to be neglected. Thus, the term (ρu) in the integration sign equals to the total mass flux G . Then Eq. (16) can be simplified as

$$\frac{2\tau_w}{R} - \frac{\tau_w - \tau_\delta}{\delta} + (\rho_b - \bar{\rho})g = \frac{G}{\delta} \frac{d}{dx} \left(\int_0^\delta u dy \right) - G \frac{du_b}{dx} \quad (17)$$

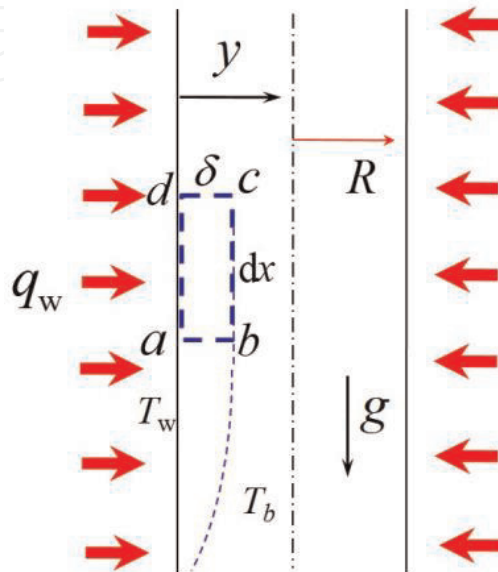


Figure 6.
Physical model of the straight tube.

Note that the thickness of the thermal boundary layer δ is negligible compared with the radius of the tube R . Concerning with this fact

$$\frac{\tau_w - \tau_\delta}{\delta} = (\rho_b - \bar{\rho})g + \left[G \frac{du_b}{dx} - \frac{G}{\delta} \frac{d}{dx} \left(\int_0^\delta u dy \right) \right] \quad (18)$$

The effects of the buoyancy and flow acceleration on the shear stress redistribution are reflected by the two terms at the right side of Eq. (18), respectively. According to Negoescu et al. [31], in the upward flow, the influence of the flow acceleration is much weaker compared with the buoyancy. In order to simplify Eq. (18), the authors adopted the assumption that the axial velocity u_b linearly varies within the thermal boundary layer thickness δ . This leads to

$$\frac{\tau_w - \tau_\delta}{\delta} = (\rho_b - \bar{\rho})g + \left[G \frac{du_b}{dx} - \frac{G}{2\delta} \left(u_b \frac{d\delta}{dx} + \delta \frac{du_b}{dx} \right) \right] \quad (19)$$

The gradient of the bulk velocity can be obtained by the analysis on the energy balance of the bulk fluid:

$$\frac{du_b}{dx} = G \frac{d(1/\rho_b)}{dT_b} \frac{dT_b}{dx} = \frac{G \beta_b}{\rho_b c_{pb}} \frac{dH_b}{dx} = \frac{4q_w \beta_b}{\rho_b c_{pb} d} \quad (20)$$

The authors made further assumption that $\delta(du_b/dx)$ in Eq. (19) is much smaller than $u_b(d\delta/dx)$. This can be interpreted as follows: the axial thickness variation of the thermal boundary layer (δ) is negligible compared with the axial bulk velocity (u_b) variation. Then Eq. (19) could be simplified as

$$\frac{\tau_w - \tau_\delta}{\tau_w} = \frac{2(\rho_b - \bar{\rho})g\delta}{f_b \rho_b u_b^2} + \frac{\delta}{f_b u_b} \frac{du_b}{dx} \quad (21)$$

Thus, the drop of the shear stress across the thermal boundary layer can be rewritten as the following pattern:

$$\frac{\tau_w - \tau_\delta}{\tau_w} = \left[\frac{2\overline{Gr}_b}{Re_b^2} + \frac{4k_T}{Re_b Pr_b} \right] \frac{\delta}{f_b d} \quad (22)$$

where \overline{Gr}_b is the average Grashof number and k_T is a nondimensional parameter reflecting the expansion of the fluid:

$$\overline{Gr}_b = \frac{\rho_b(\rho_b - \bar{\rho})gd^3}{\mu_b^2}, \quad \bar{\rho} = \begin{cases} \frac{1}{2}(\rho_w + \rho_b) & \text{for } T_w < T_{pc} \text{ or } T_b > T_{pc} \\ \frac{1}{T_w - T_b} [\rho_b(T_{pc} - T_b) + \rho_w(T_w - T_{pc})] & \text{for } T_b \leq T_{pc} \leq T_w \end{cases} \quad (23)$$

$$k_T = \frac{\beta_b q_w d}{\lambda_b} \quad (24)$$

Therefore, Eq. (22) can also be rewritten as

$$\frac{\tau_w - \tau_\delta}{\tau_w} = \left[\frac{2\overline{Gr}_b}{Re_b^2} + \frac{4\beta_b dq_w}{Re_b \mu_b c_{pb}} \right] \frac{\delta}{f_b d} \quad (25)$$

In order to build the connection between the shear stress and heat transfer, the authors analyzed the energy balance of the element $abcd$ shown in **Figure 6**:

$$q_w + \rho_b u_b \frac{d}{dx} \left(\int_0^\delta c_p T dy \right) + c_{pb} T_b \frac{d}{dx} \left(\int_0^\delta \rho u dy \right) = -\lambda_b \left(\frac{dT}{dy} \right)_{y=\delta} - \frac{\mu_t}{Pr_t} \left(\frac{\partial H}{\partial y} \right)_{y=\delta} \quad (26)$$

The physical interpretation of the budgets in the above equation can be given as follows: the first term is the wall heat flux (i.e., energy input from the boundary ad); the second term is the net energy input by the convection through the boundaries ab and cd ; the third term is the fluid energy from the core layer through the boundary bc . The axial heat conduction is ignored here. The fourth and fifth terms are the energy output by the heat conduction and turbulence diffusion through the boundary bc , respectively. As is indicated by Kurganov and Kaptil'ny [6], the turbulent viscosity in the thermal boundary layer drastically attenuates under the deteriorated HT regime. A factor $C_{\mu 1}$ is introduced here to reflect the ratio of the turbulent viscosities under the deteriorated HT regime and normal HT regime. Moreover, based on the mixing length assumption, the turbulent viscosity at the boundary bc is

$$\mu_t = C_{\mu} \rho_b l^2 \left| \frac{\partial u}{\partial y} \right|_{y=\delta} = C_{\mu} \rho_b l^2 \frac{|\tau_\delta|}{\mu_t}, \mu_t = C_{\mu 1} (\rho_b l^2 |\tau_\delta|)^{1/2} \quad (27)$$

In order to give the qualitative description of μ_t , the authors applied the Bo^* number and ρ_w/ρ_b into Eq. (27) to reflect the influence of the buoyancy force and the variable thermophysical properties:

$$C_{\mu 1} = \varphi Bo_b^{*m} \left(\frac{\rho_w}{\rho_b} \right)^n, Bo_b^* = \overline{Gr}_b / Re_b^{2.7} \quad (28)$$

where m and n are the exponents. Then the Nikuras-Van Driest mixing length model was chosen here [32]:

$$l_m/R = (0.14 - 0.08\eta^2 - 0.06\eta^4)[1 - \exp(-y^+/26)], \eta = (R - y)/R \quad (29)$$

The wall distance y^+ was taken as the dimensionless thickness of the thermal boundary layer, and it is defined as

$$y^+ = \frac{\rho_l u_\tau}{\mu_l} y = \frac{\sqrt{\rho_l \tau_w}}{\mu_l} y \quad (30)$$

For the variable-property turbulence, the local value of the thermophysical properties is more advantageous [33, 34]. Therefore, in Eq. (30) the local definitions of the density and viscosity were adopted. Considering the thermal boundary layer thickness (δ) minuteness, the authors omitted the terms higher than the second order in the Taylor series of the two terms at the right side of Eq. (26):

$$-\lambda_b \left(\frac{dT}{dy} \right)_{y=\delta} \approx \lambda_b \frac{T_w - T_b}{\delta}, -\frac{\mu_t}{Pr_t} \left(\frac{dH}{dy} \right)_{y=\delta} \approx \frac{\mu_t}{Pr_t} \frac{H_w - H_b}{\delta} \quad (31)$$

The terms on the left side of Eq. (26) can be dealt as follows:

$$\rho_b u_b \frac{d}{dx} \left(\int_0^\delta c_p T dy \right) \approx \rho_b u_b \frac{d}{dx} (H_{ave} \delta) = G \left(\delta \frac{dH_{ave}}{dx} + H_{ave} \frac{d\delta}{dx} \right) \quad (32)$$

$$c_{pb} T_b \frac{d}{dx} \left(\int_0^\delta \rho u dy \right) = GH_b \frac{d\delta}{dx} \quad (33)$$

where H_{ave} is the average specific enthalpy across the thermal boundary layer. Then the heat transfer coefficient can be obtained based on Eq. (26):

$$h = \frac{\lambda_b}{\delta} + \frac{\mu_t \bar{c}_p}{Pr_t \delta} - \frac{G}{T_w - T_b} \left(\delta \frac{dH_{ave}}{dx} + H_{ave} \frac{d\delta}{dx} + H_b \frac{d\delta}{dx} \right) \quad (34)$$

The μ_t in Eq. (26) is determined by Eq. (25) and Eqs. (20)–(22). The fitting curve among $C_{\mu 1}$, Bo^* number, and the density ratio (ρ_w/ρ_b) is obtained by the dataset of the vertically upward water flow in the circular tube under the deteriorated HT reported by Mokry et al. [9], Hu [27], Wen [35], and Wang et al. [36]. The total number of the data points is 700, with 495 data points as the fitting set and 205 data points as the assessment set. The parameters range of the dataset is given in **Table 2**.

In Eq. (26), the thermal boundary layer thickness δ is expressed as

$$\delta = \frac{\mu_b}{\sqrt{\rho_b \tau_w}} \delta^+ \quad (35)$$

According to the analysis on the temperature profiles based on the data presented in the Ref. [29] which has similar working conditions, the dimensionless excess temperature exceeds 0.9 at $\delta^+ = 300$ in the tube turbulence (for details, see Ref. [11]). For simplicity, the authors assumed an approximate value of 300 for δ^+ , and then the expression of δ can be expressed as

$$\delta = \delta^+ \mu_b / \sqrt{\rho_b \tau_w} = 300 \mu_b / \sqrt{\rho_b \tau_w} \quad (36)$$

According to Eqs. (36), (13), and (14), it can be found that the thickness of the thermal boundary layer $\delta = 300 \mu_b / \sqrt{\rho_b \tau_w} \sim 10^{-4}$ m is $R \approx 100\delta$. Thus, the assumption that the thermal boundary layer thickness is negligible compared with the tube radius is reasonable. The order of magnitude of the terms in Eq. (19) is listed as follows based on the dataset:

$$u_b \sim 1 \text{ m s}^{-1}, G \sim 10^3 \text{ kg m}^{-2} \cdot \text{s}^{-1}, \delta = 300 \mu_b / \sqrt{\rho_b \tau_w} \sim 10^{-4} \text{ m}, \quad (37)$$

$$\frac{d\delta}{dx} = 1321 G^{-0.875} d^{0.125} \mu^{-0.125} \frac{d\mu}{dT} \frac{dT_b}{dx} \sim 10^{-6}, u_b \frac{d\delta}{dx} \sim 10^{-6} \text{ m s}^{-1}$$

Refs.	P (MPa)	G (kg m ⁻² s ⁻¹)	q (kW m ⁻²)	d (mm)	H_b (kJ kg ⁻¹)	Heated length (m)
Mokry et al. [9]	24.1	129–334	200–500	10	1450–2600	4.0
Hu [27]	23–30	300–500	600–900	26	1300–2900	2.0
Wen [35]	23–26	332–700	446–600	7.6	1300–2900	2.64
Wang et al. [36]	23	450–536	450–458	10	1300–2400	2.5

Table 2.
 The experimental data sources used in the paper.

$$\begin{aligned} q_w &\sim 5 \times 10^5 \text{ W m}^{-2}, \rho_b \sim 5 \times 10^2 \text{ kg m}^{-3}, d \sim 10^{-2} \text{ m}, \\ \beta &\sim 10^{-1} \text{ K}^{-1}, c_p \sim 10^4 \text{ J kg}^{-1} \text{ K}^{-1}, \frac{du_b}{dx} \sim 1 \text{ s}^{-1}, \delta \frac{du_b}{dx} \sim 10^{-4} \end{aligned} \quad (38)$$

The authors got that the $u_b(d\delta/dx)$ could be ignored compared with the term $\delta(du_b/dx)$. Therefore, the assumption simplifying Eq. (19) is reasonable. Similarly, the order of magnitude of the parameters in Eqs. (32) and (33) could be analyzed as follows:

$$\begin{aligned} G &\sim 10^3 \text{ kg m}^{-2} \text{ s}^{-1}, q_w \sim 5 \times 10^5 \text{ W m}^{-2}, \\ H &\sim 10^6 \text{ J kg}^{-1}, d \sim 10^{-2} \text{ m}, \frac{dH_{ave}}{dx} \approx \frac{dH_b}{dx} = \frac{4q_w}{Gd} \sim 10^5 \text{ J kg}^{-1} \end{aligned} \quad (39)$$

$$\delta = 300\mu_b/\sqrt{\rho_b\tau_w} \sim 10^{-4} \text{ m}, \frac{d\delta}{dx} = 1321G^{-0.875}d^{0.125}\mu^{-0.125}\frac{d\mu}{dT}\frac{dT_b}{dx} \sim 10^{-6} \quad (40)$$

Therefore,

$$\rho_b u_b \frac{d}{dx} \left(\int_0^\delta c_p T dy \right) \approx G \left(\delta \frac{dH_{ave}}{dx} + H_{ave} \frac{d\delta}{dx} \right) \sim 10^4 \text{ W m}^{-2} \quad (41)$$

$$c_{pb} T_b \frac{d}{dx} \left(\int_0^\delta \rho u dy \right) = GH_b \frac{d\delta}{dx} \sim 10^3 \text{ W m}^{-2} \quad (42)$$

The second and third terms at the left side of Eq. (26) are far less than the q_w in the left side; thus, they could also be ignored. Eq. (34) could be simplified as

$$h = \frac{\lambda_b}{\delta} + \frac{\mu_t \bar{c}_p}{\text{Pr}_t \delta} \quad (43)$$

Plugging Eqs. (25), (27)–(30), and (36) into Eq. (43), the final form of the model could be obtained after some arrangements:

$$\text{Nu}_b = C_A \text{Re}_b^{0.875} \left\{ 1 + C_{\mu 1} C_B \text{Re}_b^{0.875} \frac{\bar{\text{Pr}}_b}{\text{Pr}_t} \left(\frac{l_m}{d} \right) \left| 1 - C_d \left(\frac{2\overline{\text{Gr}}_b}{\text{Re}_b^{2.625}} + \frac{4k_T}{\text{Re}_b^{1.625} \text{Pr}_b} \right) \right|^{0.5} \right\} \quad (44)$$

where $C_A = 6.67 \times 10^{-4}$, $C_B = 0.2$, $C_d = 1.9 \times 10^4$, $\text{Pr}_t = 0.9$. The fitting equation of $C_{\mu 1}$ was obtained as follows:

For $3 \times 10^{-6} < \text{Bo}_{\max}^* < 8 \times 10^{-5}$,

$$C_{\mu 1} = 1.115 \text{Bo}_b^{*0.147} (\rho_w/\rho_b)^{1.365} \quad (45)$$

For $8 \times 10^{-5} < \text{Bo}_{\max}^* < 3 \times 10^{-4}$,

$$C_{\mu 1} = 0.0016 \text{Bo}_b^{*-0.416} (\rho_w/\rho_b)^{1.325} \quad (46)$$

Here the parameter Bo_{\max}^* is defined as the maximum of the buoyancy number (Bo^*) under a specified case (i.e., specified P , G , q_w , d). The range of the parameters in the new correlation is $P = 23\text{--}30 \text{ MPa}$, $G = 200\text{--}900 \text{ kg m}^{-2} \text{ s}^{-1}$, $q = 129\text{--}700 \text{ kW m}^{-2}$, $d = 7.6\text{--}26 \text{ mm}$, $3 \times 10^{-6} < \text{Bo}_{\max}^* < 3 \times 10^{-4}$.

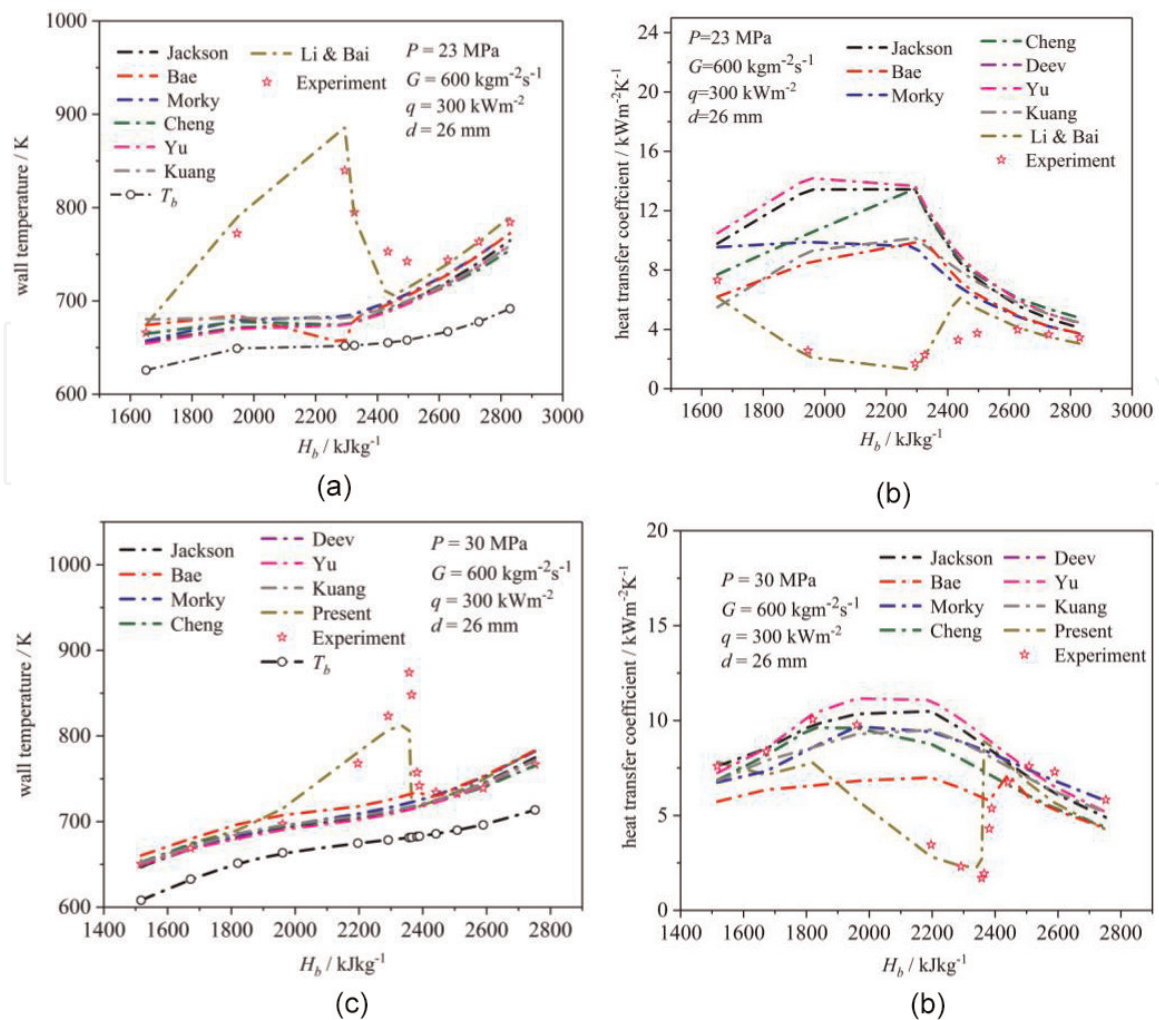


Figure 7. Comparisons of the predicted results and experimental results. Experimental data come from Hu [27], as is shown in Table 2; (a) and (c) are the wall temperature results; (b) and (d) are the heat transfer coefficients results. Data in this figure come from Ref. [11].

Figure 7 depicts the results of the model evaluation based on the above assessing procedure. It is clear that all the existing correlations could not obtain the tendencies of the wall temperature under the heat transfer deterioration regime. The semiempirical model proposed by Li and Bai shows comparatively higher accuracy compared with the existing correlations, especially at the peak region of the wall temperature. Most of the existing correlations significantly overestimate the heat transfer coefficients under the heat transfer deterioration regime.

In Figure 8, the error graphs of different heat transfer correlations (here the fitting set and the assessment set are both included) are shown. It is shown that the semiempirical correlations introduced here are correlated well with the heat transfer coefficients dataset. Seventy-two percent and 63% of the data points fall into the error bars of $\pm 30\%$ and $\pm 25\%$, respectively. In order to further investigate the predicting capacity under the deteriorated HT regime, the authors introduced another two statistical parameters: the mean relative error (*MRE*) and the root mean square error (*RMSE*) to evaluate the different correlations performance. Their definitions are given in Eqs. (47)–(49), and the comparison results are shown in Table 3. As can be seen, the Li and Bai correlation can give the smallest prediction errors, thus proving its suitability and superiority.

$$RE_i = \frac{|EXP_i - PRE_i|}{EXP_i} \quad (47)$$

$$MRE = \frac{1}{n} \sum_{i=1}^n |RE_i| \quad (48)$$

$$RMSE = \sqrt{\frac{1}{n} \sum_{i=1}^n (RE_i^2)} \quad (49)$$

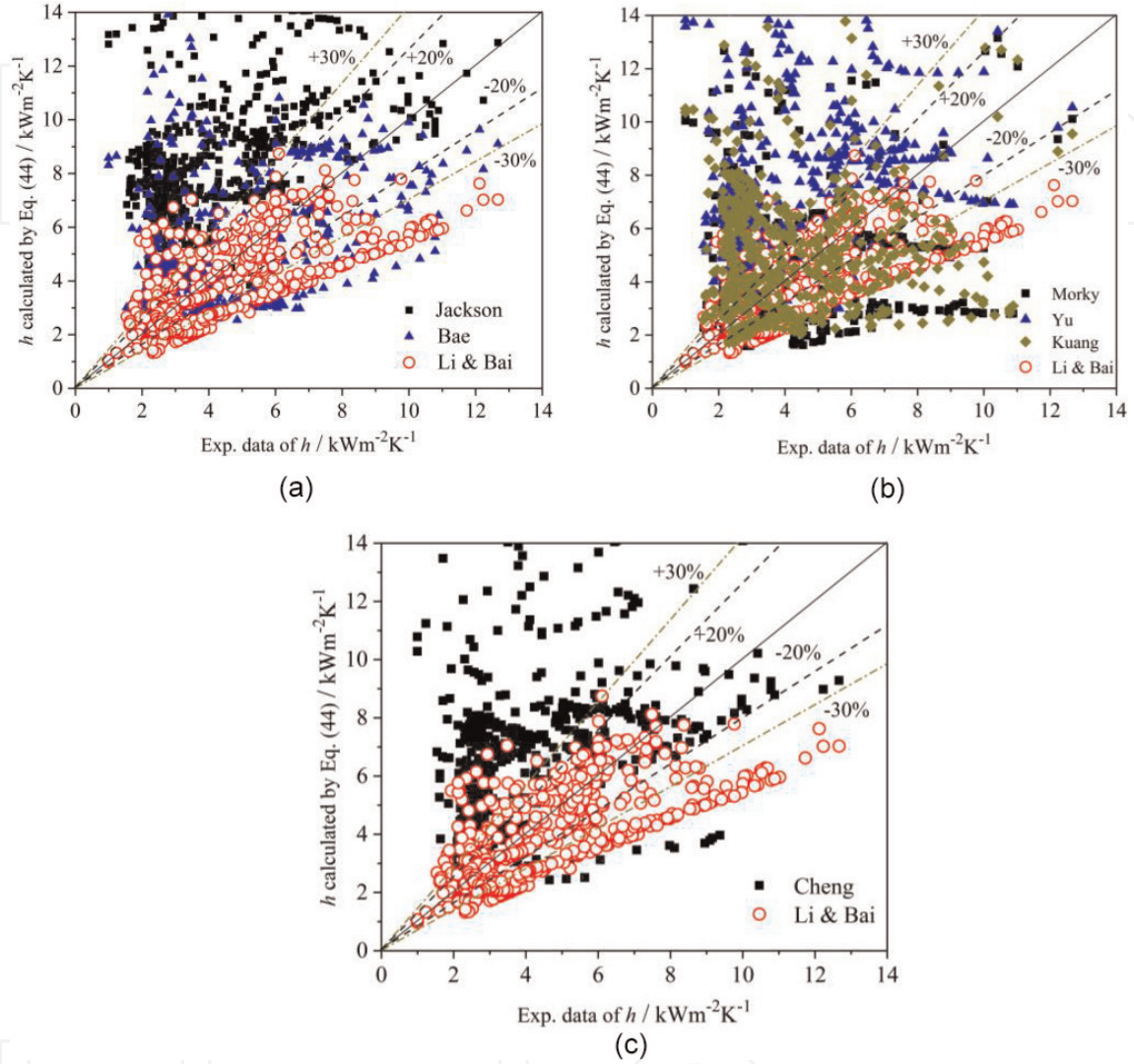


Figure 8. The errors of the predicted results of different heat transfer correlations. Data in this figure come from Ref. [11]. (a) comparison among Jackson correlation, Bae correlation and Li & Bai correlation; (b) comparison among Morky correlation, Yu correlation, Kuang correlation and Li & Bai correlation; (c) comparison between Cheng correlation and Li & Bai correlation.

Correlation	MRE/%	RMSE/%
Mokry et al. [9]	44	96
Bae et al. [10]	63	279
Jackson [23]	130	180
Cheng et al. [20]	94	148
Yu et al. [21]	10	163
Kuang et al. [22]	65	113
Li and Bai [11]	27	32

Table 3. The statistics of the present and existing correlations.

4. Conclusions

The approach to establishing the heat transfer correlations of supercritical fluids is a critical issue since the correlations play very important role in the design and optimization of the systems and devices. In this chapter, we have discussed the principles and applications of the heat transfer correlations of supercritical fluids. The modeling approaches of the correlations of supercritical fluid heat transfer are reviewed, including the nondimensional parameters applied on the modification of the empirical correlations and the “equivalent buoyancy-free flow method” used for the semiempirical correlations.

Then we introduce a new physically based semiempirical correlation which is based on the momentum and energy conservations in the mixing convective flow. Considering the mechanism of heat transfer deterioration, a physical model characterizing the redistribution of the shear stress under the combined effect of buoyancy and flow acceleration was obtained. Then the model about the heat transfer coefficients under the influence of the reduced shear stress was derived by the energy integration equation within the thermal boundary layer. Based on this, a semiempirical heat transfer correlation was proposed and then verified with a wide range of experimental data. Compared with the existing correlations, the prediction accuracy of this newly developed correlation is significantly improved under the heat transfer deterioration regime. The investigation on the different statistical parameters shows that this semiempirical correlation is superior to the empirical ones.

Acknowledgements

This study is supported by the National Key Research and Development Program of China (no. 2016YFB0600100) and the China National Funds for Distinguished Young Scientists (no. 51425603).

Conflict of interest

No conflict.

Abbreviations

DB	Dittus-Bolter
DNS	direct numerical simulation
EXP	experimental results
HT	heat transfer
MRE	mean relative error
PRE	results given by correlations
RE	relative error
RSME	root mean square error

Appendices and nomenclature

Ac	flow acceleration parameter
Bo*	Jackson buoyancy parameter

Bo_m^*	the maximum Jackson buoyancy number under a specified working condition
Bu	Bae and Kim buoyancy parameter
c_1, c_2, c_k	exponents in the empirical correlations (in Figure 2)
c_p	specific heat ($J\ kg^{-1}\ K^{-1}$)
\bar{c}_p	average specific heat in the thermal boundary layer ($= (H_w - H_b)/(T_w - T_b)$) ($J\ kg^{-1}\ K^{-1}$)
$C_\mu, C_{\mu 1}$	the correction coefficients under heat transfer deterioration in the Li and Bai correlation
$C_A, C_B, C_{\mu 1}, C_d, m, n$	constants in the Li and Bai correlation
d	inside diameter of the circular tube (m)
f	Fanning resistance coefficient
F, F_1, F_2	constants in the Cheng correlation
$F'_{VP1}, F'_{VP2}, F'_{VP3}$	the modifications on the variable properties for the “equivalent” buoyancy-free flow
$F_{VP1}, F_{VP2}, F_{VP3}$	the modifications on the variable properties for the real flow
F_{VPA}	the modification on the variable properties for the acceleration-influenced flow
F_{VPB}	the modification on the variable properties for the buoyancy-influenced flow
g	gravitational acceleration ($m\ s^{-2}$)
G	mass flux ($kg\ m^{-2}\ s^{-1}$)
Gr	Grashof number
h	local heat transfer coefficient ($kW\ m^{-2}\ K^{-1}$)
H	enthalpy ($kJ\ kg^{-1}$)
k_T	the dimensionless number reflecting the expansion of the fluid
l_m	the mixing length (m)
m_1, m_2, m_4, n_2	the exponents in the Jackson’s semiempirical model
Nu	Nusselt number
P	pressure (MPa)
Pr	Prandtl number
\overline{Pr}_b	average Prandtl number across the thermal boundary layer
Pr_t	turbulent Prandtl number
q	wall heat flux ($kW\ m^{-2}$)
r	radial coordinate (m)
R	tube radius (m)
Re	Reynolds number
T	temperature (K)
X, Y	nondimensional parameters in the empirical correlation (in Figure 2)
$Y, Y_1, Y_2, K_h, K_{Am}, K_{qm}$	constants in the Deev correlation
y	distance from the wall (m)
y^+	nondimensional distance from the wall

Greek symbols

λ	thermal conductivity ($W\ m^{-1}\ K^{-1}$)
β	thermal expansion rate (K^{-1})
ρ	density ($kg\ m^{-3}$)
μ	dynamic viscosity (Pa s)

δ	thermal boundary layer thickness (m)
δ^+	nondimensional thermal boundary layer thickness in wall units
θ	nondimensional excess temperature
φ	the constant in the Li and Bai correlation
ψ	the functional expression for the acceleration-influenced or buoyancy-influenced heat transfer
τ	shear stress (Pa)

Superscripts

T	transpose matrix
-----	------------------

Subscripts

A	flow acceleration effect
ave	average value over the thermal boundary layer
B	buoyancy effect
BA	combined effect of the buoyancy and flow acceleration
b	bulk value
max	maximum
F, f	forced convection
l	definition based on the local values
t	turbulence
pc	pseudo-critical point
w	values at the wall

Author details

Fangbo Li, Binbin Pei and Bofeng Bai*
State Key Laboratory of Multiphase Flow in Power Engineering, Xi'an Jiaotong University, Xi'an, China

*Address all correspondence to: bfbai@mail.xjtu.edu.cn

IntechOpen

© 2019 The Author(s). Licensee IntechOpen. This chapter is distributed under the terms of the Creative Commons Attribution License (<http://creativecommons.org/licenses/by/3.0>), which permits unrestricted use, distribution, and reproduction in any medium, provided the original work is properly cited. 

References

- [1] Zhang Q, Li HX, Zhang WQ, Li LX, Lei XL. Experimental study on heat transfer to the supercritical water upward flow in a vertical tube with internal helical ribs. *International Journal of Heat and Mass Transfer*. 2015; **89**:1044-1053. DOI: 10.1016/j.ijheatmasstransfer.2015.05.109
- [2] Guo LJ, Jin H, Lu YJ. Supercritical water gasification research and development in China. *Journal of Supercritical Fluids*. 2015; **96**:144-150. DOI: 10.1016/j.supflu.2014.09.023
- [3] Zhao Z, Su S, Si N, Hu S, Wang Y, Xu J, et al. Exergy analysis of the turbine system in a 1000 MW double reheat ultra-supercritical power plant. *Energy*. 2017; **119**:540-548. DOI: 10.1016/j.energy.2016.12.072
- [4] Li ZH, Wu YX, Tang GL. Comparison between heat transfer to supercritical water in a smooth tube and in an internally ribbed tube. *International Journal of Heat and Mass Transfer*. 2015; **84**:529-541. DOI: 10.1016/j.ijheatmasstransfer.2015.01.047
- [5] Bae YY, Kim HY, Kang DJ. Forced and mixed convection heat transfer to supercritical CO₂ vertically flowing in a uniformly-heated circular tube. *Experimental Thermal and Fluid Science*. 2010; **34**:1295-1308. DOI: 10.1016/j.expthermflusci.2010.06.001
- [6] Kurganov VA, Kaptil'ny AG. Velocity and enthalpy fields and eddy diffusivities in a heated supercritical fluid flow. *Experimental Thermal and Fluid Science*. 1992; **5**:465-478. DOI: 10.1016/0894-1777(92)90033-2
- [7] Bae JH, Yoo JY, McEligot DM. Direct numerical simulation of heated CO₂ flows at supercritical pressure in a vertical annulus at Re = 8900. *Physics of Fluids*. 2008; **20**:055108. DOI: 10.1063/1.2927488
- [8] Bae JH, Yoo JY, Choi H. Direct numerical simulation of turbulent supercritical flows with heat transfer. *Physics of Fluids*. 2005; **20**:105104. DOI: 10.1063/1.2047588
- [9] Mokry S, Pioro IL, Farah A, King K, Gupta S, Peiman W, et al. Development of supercritical water heat-transfer correlation for vertical bare tubes. *Nuclear Engineering and Design*. 2011; **241**:1126-1136. DOI: 10.1016/j.nucengdes.2010.06.012
- [10] Bae YY, Kim HY. Convective heat transfer to CO₂ at a supercritical pressure flowing vertically upward in tubes and an annular channel. *Experimental Thermal and Fluid Science*. 2009; **33**:329-339. DOI: 10.1016/j.expthermflusci.2008.10.002
- [11] Li FB, Bai BF. A model of heat transfer coefficient for supercritical water considering the effect of heat transfer deterioration. *International Journal of Heat and Mass Transfer*. 2019; **133**:316-329. DOI: 10.1016/j.ijheatmasstransfer.2018.12.121
- [12] Jackson JD. Models of heat transfer to fluids at supercritical pressure with influences of buoyancy and acceleration. *Applied Thermal Engineering*. 2017; **124**:1481-1491. DOI: 10.1016/j.applthermaleng.2017.03.146
- [13] Yamagata K, Nishikawa K, Hasegawa S, Fujii T, Yoshida S. Forced convective heat transfer to supercritical water flowing in tubes. *International Journal of Heat and Mass Transfer*. 1972; **15**:2575-2593. DOI: 10.1016/0017-9310(72)90148-2
- [14] Vikhrev YV, Barulin YD, Kon'Kov AS. A study of heat transfer in

- vertical tubes at supercritical pressures. *Thermal Engineering*. 1967;**14**(9): 116-119
- [15] Pioro IL, Khartabil HF, Duffey RB. Heat transfer to supercritical fluids flowing in channels-empirical correlations (survey). *Nuclear Engineering and Design*. 2004;**230**: 69-91. DOI: 10.1016/j.nucengdes.2003.10.010
- [16] Gupta S, Farah A, King K, Mokry S, Pioro I. Developing new heat-transfer correlation for supercritical-water flow in vertical bare tubes. In: *Proceedings of ICONE-18*; 17–21 May 2010; Xi'an, China.
- [17] Yoo JY. The turbulent flows of supercritical fluids with heat transfer. *Annual Review of Fluid Mechanics*. 2013;**45**:495-525. DOI: 10.1146/annurev-fluid-120710-101234
- [18] Komita H, Morooka S, Yoshida S, Mori H. Study on the heat transfer to the supercritical pressure fluid for supercritical water cooled power reactor development. In: *Proceedings of the NURETH-10*, 2005; Seoul, Korea
- [19] Deev VI, Kharitonov VS, Baisov AM, Churkin AN. Universal dependencies for the description of heat transfer regimes in turbulent flow of supercritical fluids in channels of various geometries. *Journal of Supercritical Fluids*. 2018;**135**:160-167. DOI: 10.1016/j.supflu.2018.01.019
- [20] Cheng X, Yang YH, Huang SF. A simplified method for heat transfer prediction of supercritical fluids in circular tubes. *Annals of Nuclear Energy*. 2009;**36**:1120-1128. DOI: 10.1016/j.anucene.2009.04.016
- [21] Yu J, Jia B, Wu D, Wang D. Optimization of heat transfer coefficient correlation at supercritical pressure using genetic algorithms. *Heat and Mass Transfer*. 2009;**45**:757-766. DOI: 10.1007/s00231-008-0475-4
- [22] Kuang B, Zhang Y, Cheng X. A wide-ranged heat transfer correlation of water at supercritical pressures in vertical upward tubes. In: *Proceedings of the China-Canada Joint Workshop on SCWR*, 2008; Shanghai
- [23] Jackson JD. Fluid flow and convective heat transfer to fluids at supercritical pressure. *Nuclear Engineering and Design*. 2013;**264**: 24-40. DOI: 10.1016/j.nucengdes.2012.09.040
- [24] Schatte GA, Kohlhepp A, Wieland C, Spliethoff H. Development of a new empirical correlation for the prediction of the onset of the deterioration of heat transfer to supercritical water in vertical tubes. *International Journal of Heat and Mass Transfer*. 2016;**102**:133-141. DOI: 10.1016/j.ijheatmasstransfer.2016.06.007
- [25] Koshizuka S, Takano N, Oka Y. Numerical analysis of deterioration phenomena in heat transfer to supercritical water. *Transactions of the JSME*. 1995;**38**:3077-3084. DOI: 10.1016/0017-9310(95)00008-W
- [26] Cheng X, Kuang B, Yang YH. Numerical analysis of heat transfer in supercritical water cooled flow channels. *Nuclear Engineering and Design*. 2007;**237**:240-252. DOI: 10.1016/j.nucengdes.2006.06.011
- [27] Hu ZH. Heat transfer characteristics of vertical upflow and inclined tube in the supercritical pressure and near-critical pressure region [thesis]. Xi'an: Xi'an Jiaotong University; 2001
- [28] Peeters JW, Pecnik R, Rohde M, et al. Turbulence attenuation in simultaneously heated and cooled annular flows at supercritical pressure.

Journal of Fluid Mechanics. 2016;**799**:
505-540. DOI: 10.1017/jfm.2016.383

[29] Zhang G, Zhang H, Gu H, Yang Y, Cheng X. Experimental and numerical investigation of turbulent convective heat transfer deterioration of supercritical water in vertical tube. Nuclear Engineering and Design. 2012; **248**:226-237. DOI: 10.1016/j.nucengdes.2012.03.026

[30] Kim DE, Kim MH. Two layer heat transfer model for supercritical fluid flow in a vertical tube. Journal of Supercritical Fluids. 2011;**58**:15-25. DOI: 10.1016/j.supflu.2011.014.

[31] Negoescu CC, Li Y, Al-Duri B, Ding Y. Heat transfer behavior of supercritical nitrogen in the large specific heat region flowing in a vertical tube. Energy. 2017;**134**:1096-1106. DOI: 10.1016/j.energy.2017.04.047

[32] Patankar SV, Ivanovic M, Sparrow EM. Analysis of turbulent flow and heat transfer in internally finned tubes and annuli. Journal of Heat Transfer-Transactions of the ASME. 1979;**101**:29-42. DOI: 10.1115/1.3450925

[33] Chu X, Laurien E, McEligot DM. Direct numerical simulation of strongly heated air flow in a vertical pipe. International Journal of Heat and Mass Transfer. 2016;**101**:1163-1176. DOI: 10.1016/j.ijheatmasstransfer.2016.05.038

[34] Huang PG, Coleman GN, Bradshaw P. Compressible turbulent channel flows: DNS results and modelling. Journal of Fluid Mechanics. 1995;**305**:185-218. DOI: 10.1017/S0022112095004599

[35] Wen QL. Experimental study of flow and heat transfer characteristics at SCWR typical conditions [thesis]. Shanghai, Shanghai Jiao Tong University; 2015

[36] Wang F, Yang J, Gu H, Zhao M, Li H, Lu D. Experimental research on heat transfer performance of supercritical water in vertical tube. Atomic Energy Science and Technology. 2013;**47**:933-939